energy&fuels

Article

pubs.acs.org/EF

High-Pressure Methane Adsorption and Characterization of Pores in Posidonia Shales and Isolated Kerogens

Thomas F. Rexer,[†] Eliza J. Mathia,[†] Andrew C. Aplin,[‡] and K. Mark Thomas*[,†]

[†]Wolfson Northern Carbon Reduction Laboratories, School of Civil Engineering and Geosciences, and School of Chemical Engineering and Advanced Materials, Drummond Building, Newcastle University, Newcastle upon Tyne, NE1 7RU, United Kingdom

[‡]Department of Earth Sciences, Durham University, Science Laboratories, Durham, DH1 3LE, United Kingdom

Supporting Information

ABSTRACT: Sorption capacities and pore characteristics of bulk shales and isolated kerogens have been determined for immature, oil-window, and gas-window mature samples from the Lower Toarcian Posidonia shale formation. Dubinin–Radushkevich (DR) micropore volumes, sorption pore volumes, and surface areas of shales and kerogens were determined from CO_2 adsorption isotherms at −78 and 0 °C, and from N_2 adsorption isotherms at −196 °C. Mercury injection capillary pressure porosimetry, grain density measurements, and helium pycnometry were used to determine shale and kerogen densities and total pore volumes. Total porosities decrease through the oil-window and then increase into the gas-window. High-pressure methane isotherms up to 14 MPa were determined at 45, 65, and 85 °C on dry shale and at 45 and 65 °C on kerogen. Methane excess uptakes at 65 °C and 11.5 MPa were in the range 0.056–0.110 mmol g^{-1} (40–78 scf t^{-1}) for dry Posidonia shales and 0.36–0.70 mmol g^{-1} (253–499 scf t^{-1}) for the corresponding dry kerogens. Absolute methane isotherms were calculated by correcting for the gas at bulk gas phase density in the sorption pore volume. The enthalpies of CH_4 adsorption for shales and kerogens at zero surface coverage showed no significant variation with maturity, indicating that the sorption pore volume is the primary control on sorption uptake. The sum of pore volumes measured by (a) CO_2 sorption at −78 °C and (b) mercury injection, are similar to the total porosity for shales. Since mercury in our experiments occupies pores with constrictions larger than ca. 6 nm, we infer that porosity measured by CO_2 adsorption at −78 °C in the samples used in this study is largely within pores with effective diameters smaller than 6 nm. The linear correlation between maximum CH_4 surface excess sorption and CO_2 sorption pore volume at −78 °C is very strong for both shales and kerogens, and goes through the origin, suggesting that the vast majority of sorbed CH_4 occurs in pores smaller than 6 nm. The DR micropore volume obtained from CO_2 adsorption at 0 °C was 40%–62% of the corresponding CO_2 sorption pore volume. Sorption mass balances using kerogen and shale isotherms showed that approximately half of the CO_2 sorption in these dry shales is in organic matter, with the rest likely to be associated with the inorganic phase (mainly clay minerals). A similar distribution was observed for supercritical CH_4 adsorption. Mass balances for adsorption isotherms for kerogen and clay minerals do not always account for the total measured sorbed CH_4 on dry shales, suggesting that some sorption may not be completely accounted for by the minerals identified and kerogens in the shales.

1. INTRODUCTION

Shale gas is a key methane supply resource for the future. In 2010, it accounted for 20% of the natural gas production in the United States, up from 1% in 2000.[1] The economic potential of shale gas reservoirs is essentially a function of the Gas-in-Place (GIP) and the rate at which that gas can be supplied from the shale matrix to an induced fracture network connected to a wellbore. At the heart of both factors is the requirement to quantify the nature of the shale pore volume and to understand how variations in pore size distributions affect the location and amounts of both sorbed and homogeneous bulk ("free") gas.

Pore volumes and size distributions in shales are affected by compaction, maturity, grain size, and mineralogy.[2−7] The pore volume of shales can be determined by various techniques, such as mercury injection capillary pressure (MICP) porosimetry and grain density/helium pycnometry, scanning electron microscopy (SEM) images, and gas sorption techniques, with each method characterizing a specific pore size range. Ultra-small-angle neutron scattering and small-angle neutron scattering techniques are also useful for the determination of pore connectivity in shales.[8−10] Sorbed gas in shale is in equilibrium with the homogeneous bulk gas phase ("free gas") in larger pores. Sorption capacity depends on pressure and temperature, and structural characteristics, such as (micro-) pore volume and organic matter type, maturity, and content. Supercritical methane maximum surface excess adsorption decreases linearly with reciprocal of absolute temperature for an Alum shale.[11] The hygroscopic moisture content of shales correlates with methane sorption capacity indicating that methane and water compete for the same sorption sites. Also, under geological conditions, moisture may be present leading to reduced methane capacity compared with dry shales.[12−14]

Ross et al. have reported positive correlations between maturity and sorption capacity in organic-rich shales, which they attributed to an increased micropore volume (pore width = 0.3–2 nm).[14] However, they were not able to fully explain

Received: December 15, 2013
Revised: March 27, 2014
Published: March 31, 2014

 © 2014 American Chemical Society

Table 1. Well, Sample Number, Depth, Total Organic Content (TOC), Grain and Helium Densities, Mercury Injection Pore Volumes, and Total Porosities for Posidonia Shales and Kerogens

				Shale				Kerogen	
well	sample	depth [m]	TOC [wt %]	grain density [g cm^{-3}]	density (helium pycnometry) [g cm^{-3}]	bulk volume (MICP) [cm^3 g^{-1}]	total pore volume [%]	TOC[a] [wt %]	density (helium pycnometry) [g cm^{-3}]
WIC	7145	47.4	10.92	2.331	2.321	0.497	13.8	73	1.217
WIC	7155	57.8	9.67	2.361	2.297	0.484	12.5	73	1.235
HAR	7038	44.5	7.91	2.493	2.468	0.414	3.1	97	1.168
HAR	7060	66.8	5.78	2.592	2.550	0.404	4.5	99	1.024
HAD	7090	40.1	7.41	2.572	2.556	0.439	11.4	83	1.342
HAD	7119	60.6	7.15	2.607	2.614	0.445	13.7	79	1.368

[a]The kerogen TOC content is corrected for the residual pyrite content, which could not be removed by the separation process. The pyrite removal procedure was not carried out for Harderode shales.

variations in sorption capacity by micropore volume and total organic carbon (TOC) content alone. Several authors have reported positive correlations of methane sorption uptake and TOC, implying that much of the sorbed methane in shale is associated with organic matter.[12,14,15] Gasparik et al. reported no correlation for methane sorption capacity and TOC (0.8%−10.5%) for dry shales,[16] but found a correlation for another suite of dry shales with TOC (0.4%−14.1%).[13] These results illustrate the complex nature of the problem when relating composition and structure of shales to methane sorption capacity.

The differences between surface excess and absolute amounts adsorbed become significant in high-pressure isotherms. The surface excess adsorbed represents the amount of gas exceeding bulk gas phase density in the system. The absolute amount adsorbed represents the total amount of gas molecules in the sorbed state. Various semiempirical models such as the Langmuir model or the supercritical Dubinin−Radushkevich (DR) model are available, as well as models based on density functional theory.[11,16,17] While the Langmuir models have been commonly used to parametrize shale sorption data, the supercritical DR model has been shown to have good applicability for a predominantly ultramicroporous (<0.7 nm) high-maturity Alum shale (R_0 = 2.26%), for isotherms over a wide temperature range (27−200 °C).[11] Although sorption data on shales are available, the absolute sorption capacity in shale remains poorly constrained.[11−16,18−20]

Shales are complex heterogeneous materials with amorphous kerogen and inorganic phases. The amount of methane adsorbed on shales is also very low, and this is complicated by the fact that the minor kerogen component has a much larger adsorption capacity than the inorganic phase in the shale. Previous studies have concentrated on the correlation of surface excess with geological characterization data (for example, total organic carbon, maturity, etc.), and this has significant limitations. The objective of this study was to investigate how supercritical methane sorption capacity and pore structural characteristics in shale and kerogen obtained from subcritical adsorption, change with maturity. The pore structural characteristics were obtained using subcritical carbon dioxide (−78 and 0 °C) and nitrogen (−196 °C) adsorption, mercury injection capillary pressure (MICP) porosimetry, helium pycnometry, and grain density measurements. Posidonia shale samples from the early oil-window, the oil-window and the gas-window were studied. The shale sample set is relatively homogeneous, in terms of TOC and mineral composition, allowing the impact of maturity on shale and kerogen pore structure and methane capacity to be studied independently of these variables. Kerogen samples were isolated using chemical methods. Furthermore, high-pressure methane sorption isotherms were determined on both shales and isolated kerogen to investigate the inter-relations between high-pressure sorption capacity, maturity, pore structure, and the sorbed gas distribution between organic and inorganic phases.

1.1. Posidonia Shales. The Lower Toarcian Posidonia shale is regarded as one of the most widespread and economically important petroleum source rocks of Western Europe. The formation is a reference source rock of Type II kerogen.[21−23] These black shales were deposited in an epicontinental sea of moderate depth, extending from the Yorkshire Basin (United Kingdom), over the Lower Saxony Basin and the Southwest German Basin into the Paris Basin, during the Lower Toarcian period.[21,24,25] Recent electron microscopy studies inferred that the formation of nanoporous organic materials occurred due to gaseous hydrocarbon generation in Posidonia shales of gas-window maturity.[26] Geological and geochemical history has been reviewed in detail elsewhere.[21,24−30]

2. EXPERIMENTAL SECTION

2.1. Materials. Posidonia shales were obtained from the Wickensen (WIC), Harderode (HAR), and Hadessen (HAD) boreholes. These boreholes were drilled along the Western flank of the Hils half-graben. The shales progressively increase in maturity from the early oil-window Wickensen (R_0 = 0.53%), through the mid oil-window Harderode (R_0 = 0.89%), to the gas-window Hadessen (R_0 = 1.45%) samples.[26]

Carbon dioxide and nitrogen gases were obtained from BOC with purities of 99.995% and 99.9995%, respectively. Methane, with a purity of 99.995%, was obtained from Air Products and Air Liquide.

2.2. Petrophysical Characterization. *2.2.1. Grain Density Measurements.* These measurements were carried using a glass pycnometer with a nominal volume of 50 mL. Approximately 3 g of material was crushed to <0.5 mm particle size and dried overnight at 105 °C. The sample was added to a preweighed pycnometer and weighed. Surfactant solution (10 mL) containing Teepol (5%) was added and the pycnometer was filled with degassed water and reweighed. Measurements were carried out using the British Standard methods for calibration and use of pycnometers.[31] Duplicate determinations were within 0.03 g cm^{-3}. Details of the method used for calculation of the grain densities have been given in a previous publication.[11]

2.2.2. Total Organic Carbon (TOC) Measurements. The samples were crushed to pass through a 0.5 mm sieve. Then, 0.1 g of the powder, in a porous crucible, was treated with sufficient hydrochloric acid (4 mol L^{-1}), to remove carbonates. After the acid had drained from the crucible, the crucible and sample were dried overnight at 65 °C. The total organic carbon content was then measured using a Leco Model CS244 carbon/sulfur analyzer.

dx.doi.org/10.1021/ef402466m | Energy Fuels 2014, 28, 2886−2901

Table 2. Rock Eval Pyrolysis Results for Posidonia Shales

	free hydrocarbon, S1 [mg g^{-1}]	generated hydrocarbon, S2[a] [mg g^{-1}]	temperature, T_{max}[b] [°C]	production potential, PP [mg g^{-1}]	production index, PI	hydrogen index, HI [mg_{HC} g_{TOC}^{-1}]
WIC7145	4.2	72.0	425	76.2	0.05	660
WIC7155	3.9	69.4	429	73.3	0.05	718
HAR7038	3.3	30.2	449	33.5	0.10	382
HAR7060	2.0	21.2	447	23.2	0.09	361
HAD7090	0.9	4.2	464	5.1	0.18	56
HAD7119	1.2	3.2	459	4.4	0.28	44

[a]S2 = cracked hydrocarbon through thermal cracking of nonvolatile organic matter. [b]T_{max} = temperature of maximum release of cracked hydrocarbons.

2.2.3. Rock Eval Pyrolysis. Rock Eval Pyrolysis was carried out with a Delsi Rock Eval OSA pyrolysis instrument and the following parameters were measured: *S*1 is the amount of free hydrocarbons in the sample, and *S*2 is the amount of hydrocarbons generated through thermal cracking of nonvolatile organic matter. T_{max} is the temperature of maximum release of cracked hydrocarbons. This temperature is an indicator of the maturity of the sample.[32]

2.2.4. X-ray Diffraction (XRD). The XRD data were obtained using a Siemens D5000 diffractometer, using Co Kα radiation. The samples were scanned from 2° 2θ to 75° 2θ, with a step time of 2 s per 0.02 degree step. The minerals were quantified by Hillier's method.[33,34]

2.2.5. Mercury Injection Capillary Pressure Porosimetry. Porosimetry measurements were performed using a Micromeritics Autopore IV Mercury Injection Porosimeter. Shale samples were freeze-dried for 48 h, and ∼1 cm^{-3} samples were loaded and outgassed under vacuum. The mercury pressure was increased stepwise up to 268.9 MPa. MICP bulk volumes/densities of shale were calculated from the bulk volume of the known mass of sample placed into the MICP equipment and the grain density of the sample measured by the small pycnometer method. Pore volumes, measured by injected mercury ($MICP_{pv}$), were calculated from the difference of the volume of mercury injected at 1.379 and 268.9 MPa, assuming that the small amounts of mercury injected at the lower pressure, only fill surface topography and microfractures. The macroporosity (1093−50 nm) present in some samples, which could act as methane gas storage capacity, was included in the total pore volume, but surface topography and microfractures related to the destressing and drying of geological samples were excluded (see Table 1). The Washburn equation[35] is derived for cylindrical pores, and the calculations were carried out assuming a contact angle of 141° between the mercury and the particle surface and a surface tension of 0.485 N m^{-1};[3,36,37] these values predict that, at these pressures, mercury penetrates pore throats (constrictions) with equivalent diameters between 1093 nm at 1.379 MPa and 5.6 nm at 268.9 MPa. These diameters should be regarded as equivalent pore diameters, because of the variation in pore shape in the heterogeneous shale materials. Details about the measurements are given in the Supporting Information (Section A).

2.3. Kerogen Isolation. Shales (∼25 g each) were crushed to powder and treated with 8 mL of HCl (0.5 M) to remove carbonates and acidified $CrCl_2$ (1.0 M) to remove pyrite. The mixture was diluted with degassed water. The shale particles were separated from the solution by centrifuging (15 min, 3500 min^{-1}). The process was repeated 3 times. Samples were then freeze-dried (−25 °C). Silicates were removed by treating the decarbonated and depyritized shales with 15 mL of HF (0.4 M). The process was repeated twice. The shale−acid mixture was diluted with degassed water and the kerogens were separated by filtering. For Harderode shales, no depyritization was conducted as pyrite removal proved inefficient for Wickensen and Hadessen shales. XRD profiles were obtained before and after the demineralization to ensure removal of all minerals except pyrite. Details about the process and chemical reactions are given in the Supporting Information (Section B1). The isolated kerogen samples contained varying amounts of pyrite (see Section B2, Figure S1 in the Supporting Information), which were measured by proximate analysis (see Section B3 and Table S1 in the Supporting Information). CO_2 (−78 °C) and N_2 (−196 °C) adsorption isotherms for pyrite showed that no significant adsorption occurred (see Figure S2 in the Supporting Information). Therefore, all kerogen adsorption isotherms were corrected for pyrite content (see Section B3 in the Supporting Information).

2.4. Pore Characterization by Low-Pressure Sorption. Adsorption characteristics of N_2 and CO_2 on the shales and kerogens were investigated using an Intelligent Gravimetric Analyzer (IGA), supplied by Hiden Isochema, Ltd. (Warrington, U.K.). The system has been described in detail previously.[11] Sorption measurements on shale by IGAs at temperatures above 0 °C require the removal of traces of moisture from the gas supply. Details of system modifications for moisture-removal from the gas stream are given in Section C2 in the Supporting Information.

Adsorbent samples were crushed to particle sizes between 500−1180 μm, loaded in the IGA (130−160 mg of shales, 40−105 mg of kerogens), and outgassed to a constant weight (typically for ∼4 h), at $<10^{-4}$ Pa and 110 °C. N_2 isotherms were measured at −196 °C up to a pressure of 99 kPa. CO_2 isotherms were collected at −78 and 0 °C up to 100 kPa. The saturated vapor pressure (p_0) for CO_2 at 0 °C is 3.49 MPa. All adsorption isotherms were measured a minimum of two times and the experimental repeatabilities were typically ±1.5% for CO_2 adsorption uptakes at both −78 and 0 °C at 0.1 MPa and ±1.1% for N_2 uptakes at −196 °C and 0.099 MPa.

2.5. High-Pressure Methane Sorption. High-pressure methane isotherms were measured on a Hiden Isochema Intelligent Manometric Instrument (IMI). System specifications are described in the Supporting Information (see Table S2). Crushed shale samples (500−1180 μm) and kerogens were predried (typically for ∼4 h, at <500 Pa and 110 °C) in a vacuum oven and loaded into the IMI sample cell (typically ∼10 g shale, 0.8−1.3 g kerogen). For kerogens, displacers were employed to reduce the void volume, because only relatively small quantities were available. Prior to the measurements, another internal drying was carried out (typically for ∼4 h), at $<10^{-4}$ Pa, at 110 °C followed by helium pycnometry (2 MPa dosing pressure at 40 °C and ca. 0.7 MPa at equilibrium after dosing) to determine the skeletal volume. The assumption is that helium penetrates all accessible porosity.[38]

Methane isotherms were measured at 45, 65, and 85 °C. Between measuring isotherms, the system was outgassed below $<10^{-6}$ Pa and heated to 110 °C. Excess uptake was calculated by a mass balance given in the Supporting Information (Section D1). Isotherm experimental repeatabilities were typically ±5.0% for both shale and kerogens at 10 MPa. In addition, assuming that helium adsorption is negligible, helium isotherms were measured at all temperatures as blank determinations for no adsorption, to leak-test the system and to monitor skeletal densities.

2.6. Saturated Vapor Pressure. Saturated vapor pressures (p_0) and gas densities were calculated from the NIST Standard Reference Database 23, using the REFPROP Version 9.0 software.[39] The following equations of state (EOSs) were used: CO_2 (Span et al.[40]), N_2 (Span et al.[41]), CH_4 (Setzmann et al.[42]), and helium (Lemmon et al.[39]).

Table 3. Mineral Composition of Posidonia Shales[a]

	Composition (wt %)										
	quartz	plagioclase	calcite	dolomite	pyrite	gypsum	muscovite	illite + i−s	kaolinite	chlorite	other
WIC7145	13.2	1.0	46.6	0.3	3.9	2.2	0.0	22.4	5.1	2.0	3.3
WIC7155	8.6	1.4	55.3	0.6	5.4	2.4	0.1	19.4	2.2	1.8	2.8
HAR7038	15.8	2.1	43.5	0.7	5.6	0.0	3.2	18.5	8.9	0.0	1.7
HAR7060	13.0	2.8	30.5	6.4	9.1	0.0	3.7	26.2	6.6	0.0	1.7
HAD7090	16.0	3.0	39.7	1.8	5.0	1.8	1.3	23.9	3.9	0.7	2.9
HAD7119	8.2	4.9	49.9	2.7	4.5	3.8	0.0	19.5	1.1	2.7	2.7

[a]Other minerals includes feldspar, siderite, anatase, marcasite, aragonite, and dickite (not more than 1.5 wt %).

Table 4. Shale and Kerogen Pore Volumes Measured by Different Techniques[a]

	Pore Volume [$mm^3\ g^{-1}$]							
sample	<0.7 nm CO_2 (0 °C) UMP	<1.5 nm CO_2 (0 °C) NLDFT	0.3−2 nm N_2 (−196 °C) MPV	CO_2 (−78 °C) SPV	6−1093 nm MICP	TPV	SPV+MICP	BET surface area [$m^2\ g^{-1}$]
				Shale				
WIC7145	6.7	4.6	2.9	16.4	53.1	68.4	69.5	6.7
WIC7155	8.0	7.7	1.6	15.5	48.1	60.7	63.6	4.3
HAR7038	5.2	4.3		8.4	5.1	12.7	13.5	
HAR7060	4.6	5.7		8.3	7.8	18.1	16.1	
HAD7090	6.4	6.0	11.6	16.2	26.0	50.1	42.2	25.1
HAD7119	6.0	4.0	9.1	13.0	45.1	61.1	58.1	21.0
				Kerogen				
WIC7145	32.5	21.8	5.2	74.8				12.5
WIC7155	28.8	24.3	3.7	71.8				7.5
HAR7038	27.0	25.3	11.9	68.5				27.3
HAR7060	33.5	33.1	9.0	87.0				17.9
HAD7090	50.6	42.4	34.6	113.0				68.1
HAD7119	54.6	50.8	24.2	103.6				56.1

[a]UMP = ultramicropore volume, determined using the DR equation and CO_2 sorption at 0 °C; NLDFT = pore volume determined by applying a nonlocal density functional theory model to carbon dioxide, 0 °C isotherms, N_2; MPV = micropore volume determined by the DR equation from −196 °C, nitrogen isotherms; SPV = sorption pore volume based on Gurvitch's Rule and calculated from CO_2 isotherms at −78 °C; MICP = pore volume from mercury injection capillary pressure porosimetry, the estimated pore constriction sizes were derived from the Washburn equation (see the Supporting Information); TPV = total pore volume (from eq 2), using mercury bulk density and grain density/helium pycnometry (skeletal volume); Total Porosity = 1 − mercury bulk density/(grain or He density) (eq 3) ; SPV+MICP = sum of CO_2 (−78 °C sorption) pore volume and MICP pore volume (eq 4).

3. RESULTS

3.1. Petrophysical Characterization. *Total Organic Carbon and Grain Densities.* The TOC and the grain densities obtained from both buoyancy and helium pycnometry are shown in Table 1. TOC values range from 5.8−10.9 wt %. Excellent agreement was observed for shale grain densities (2.331−2.607 g cm^{-3}) and helium pycnometry (2.297−2.614 g cm^{-3}) with measurements for specific samples agreeing within 3%. Kerogen densities were much lower and ranged from 1.024 g cm^{-3} to 1.368 g cm^{-3}.

Rock Eval Pyrolysis. The bulk geochemical data classifies the Posidonia shale kerogen as Type II with a maturation trend typical for the marine algal kerogen (see Table 2).[43] The Rock Eval analyses showed a decrease of hydrogen index (HI) from ∼700 mg HC/g in the early oil-window down to ∼370 mg HC/g in the peak oil-window and 50 mg HC/g in the gas-window. Parameters *S*1 and *S*2 decrease with increasing maturity.

The Rock Eval data for the kerogens shows that the T_{max} values are slightly lower than for the corresponding shales (see Table S1b in the Supporting Information) with the difference increasing with increasing kerogen maturity. Heat and mass-transfer effects are likely to be quite different for isolated kerogens and kerogens embedded in an inorganic shale matrix, and these factors will influence T_{max} significantly. However, good linear correlations are observed for the *S*2 peak (R^2 = 0.9595) and HI (R^2 = 0.9977) parameters for pyrolysis of the kerogen and shales (see Figures S1c and S1d in the Supporting Information). Previous work has shown that *S*2 and HI parameters are decreased by mineral matrix effects involving the retention of pyrolysis products.[44] Therefore, it is reasonable to conclude that the kerogen isolation process only had a minimal effect on kerogen properties.

Mineralogy. The bulk mineralogical compositions of these Posidonia samples are similar throughout the entire maturation sequence (see Table 3). The most abundant phases are calcite (31−55 wt %) and phyllosilicates (23−37 wt %). Within the phyllosilicates group, illite-rich mixed-layer illite−smectite is the most prominent component, followed by kaolinite, illite, muscovite, and chlorite. In addition, there is a moderate content of quartz (8−16 wt %) and minor contents of pyrite (4−9 wt %), feldspars (1−5 wt %), and dolomite (0.3−6.4 wt %). Other minerals include siderite, marcasite, and anatase, but their content does not exceed 2−3 wt %. The XRD and microscopic data classify the immature Posidonia shale as a calcareous nanoplankton-, silt-, and clay-bearing mudstone.

dx.doi.org/10.1021/ef402466m | Energy Fuels 2014, 28, 2886−2901

3.2. Pore Characterization. *3.2.1. Total Pore Volume (TPV) and MICP Pore Volume ($MICP_{pv}$).* The bulk volume obtained from MICP and the skeletal densities from grain density measurements and helium pycnometry were used to calculate the total pore volumes of the Posidonia shales. The total pore volume (<1093 nm) was obtained from mercury injection at 1.379 MPa and the helium or grain densities. Mercury injection measures the accessible pore volume for constrictions with equivalent pore widths >5.6 nm based on the prediction of the Washburn equation for the pressure (268.90 MPa) used. Correcting for conformance/surface roughness using the method of Wang et al.,[3] which, depending on the sample, ranged from 1.379 MPa to 35.2 MPa mercury pressure (corresponding to equivalent pore diameters of 43−1093 nm), did not lead to significantly different MICP pore volumes. The maximum pore sizes in the samples obtained from MICP were as follows: WIC7145, 156 nm; WIC7155, 156 nm; HAR7038, 21 nm; HAR 7060, 24 nm; HAD 7090, 156 nm; and HAD7199, 547 nm. These maximum pore sizes decrease through the oil-window and then increase into the gas-window.

Mercury injection volumes were ∼80% of total pore volumes in the Wickensen samples, ∼40% in the Harderode samples, and 50%−75% in the Hadessen samples. Total pore volumes and mercury injection volumes show the same trend with maturity (see Table 4). There is a decrease in total pore volume from ∼65 $mm^3\ g^{-1}$ to 15 $mm^3\ g^{-1}$ for the Wickensen samples (R_0 = 0.53%) to the Harderode samples (R_0 = 0.89%) and an increase back to ∼55 $mm^3\ g^{-1}$ for Hadessen (R_0 = 1.45%) shales. A similar trend of pore volume with maturity, with a minimum in the oil-window, has been observed previously for coals.[45]

3.2.2. Sorption Pore Volumes. According to the Gurvitch Rule adsorption uptake at $p/p_0 \approx 1$ when expressed as a volume of liquid, using the liquid density should be the same for all adsorptives on a given adsorbent.[46−48] These sorption pore volumes can thus be calculated from CO_2 isotherms at 0.1 MPa and −78 °C or nitrogen adsorption isotherms at 0.1 MPa and −196 °C.

Carbon dioxide isotherms for both shales and kerogens at −78 °C do not reach plateaus and are therefore classified as Type I/II in the IUPAC Classification Scheme (see Figures 1 and 2).[49] Maximum uptake (at $p/p_0 \approx 1$) was 0.23−0.44 mmol g^{-1} on shales and 1.83−3.02 mmol g^{-1} on kerogens (see Figure 1 and 2). Tabulated isotherm data are given in Supporting Information (Table S4). Normalizing the isotherms by maximum uptake reveals that all isotherms (shale and kerogen) have very similar isotherm shapes. This indicates that the Posidonia shales and kerogens have similar pore size distributions within the porosity range measured by CO_2 adsorption at −78 °C.

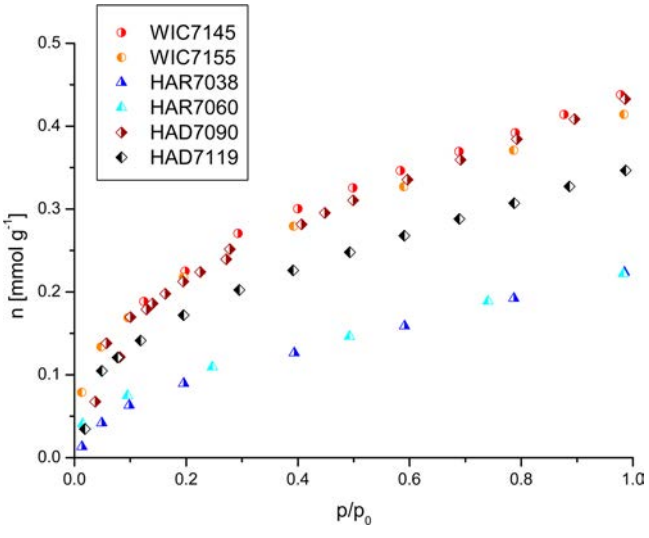

Figure 1. CO_2 adsorption isotherms for shales at −78 °C.

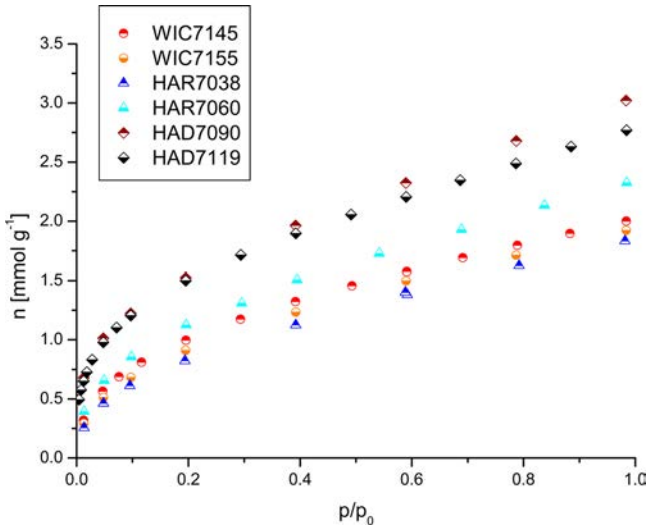

Figure 2. CO_2 isotherms for kerogens at −78 °C.

Calculated sorption pore volumes from CO_2 isotherms at −78 °C (CO_2 SPV) of shale and kerogen are shown in Table 4. An adsorbed phase density of 1.177 g cm^{-3} was assumed. There is a range of possible values for densities of adsorbed CO_2 from 1.562 g cm^{-3} for solid at −78 °C to 0.762 g cm^{-3} at 21.1 °C. The density chosen is in the middle of this range and is the liquid density of CO_2 at the boiling point (−56.6 °C).[39] CO_2 sorption pore volumes range from 8.3 $mm^3\ g^{-1}$ to 16.4 $mm^3\ g^{-1}$ on shale and from 68.5 $mm^3\ g^{-1}$ to 113.0 $mm^3\ g^{-1}$ on kerogen (see Table 4). There is a trend in sorption and MICP pore volumes with maturity with the minimum observed for HAR shales. The sum of the CO_2 sorption pore volumes and MICP pore volumes are very similar to the corresponding total pore volumes calculated from the MICP bulk volume (<1093 nm) and the grain or helium density with a linear correlation coefficient with $R^2 > 0.97$ (see Figure 3). Therefore, the CO_2 sorption pore volume and MICP pore volume (5.6−1093 nm) account for the total pore volume (<1093 nm) in this suite of shale samples. Considering that the Washburn equation is derived using cylindrical pores and predicts that mercury penetrates pore constrictions down to effective pore diameters of ∼5.6 nm, the good agreement suggests that the CO_2 sorption pore volume accounts for pores up to approximately this pore diameter. This sorption pore volume represents ∼25% of total pore volume in the Wickensen samples, 46% and 66% in the Harderode samples, and ∼21% and 32% in the Hadessen samples (see Table 4). However, we note that the high pressures used in mercury injection porosimetry may distort shale samples. Furthermore, MICP measurements were carried out on 1 cm^3 chips while sorption measurements were carried out on particles (500−1180 μm) and, thus, the accessible pore volume may differ.

dx.doi.org/10.1021/ef402466m | Energy Fuels 2014, 28, 2886−2901

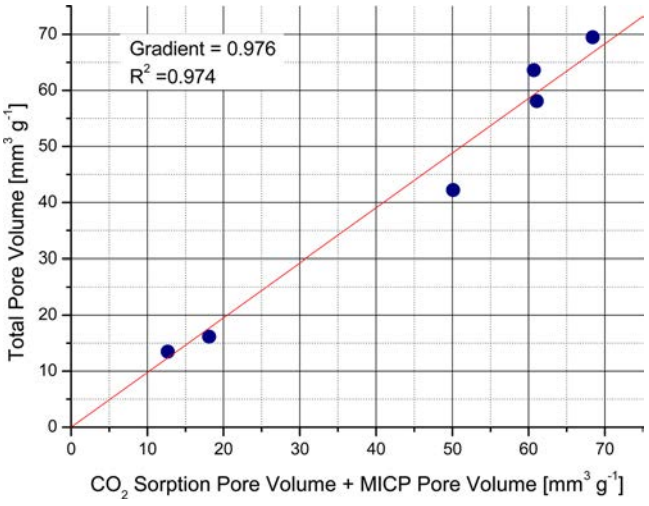

Figure 3. Correlation of total pore volume with CO_2 sorption pore volume (−78 °C) plus MICP (SVP+MICP) pore volume. Pore volumes were calculated assuming an adsorbed phase density of 1.177 g cm^{-3}.

Nitrogen adsorption isotherms of shales and kerogen at −196 °C are shown in Figures 4 and 5, respectively. Tabulated

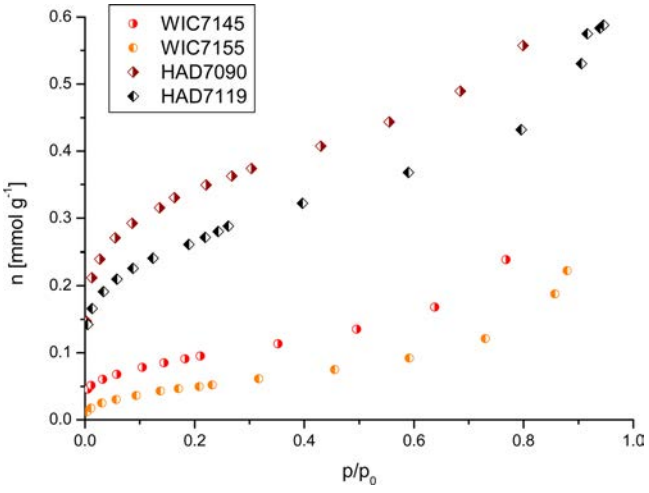

Figure 4. N_2 adsorption isotherms at −196 °C for Posidonia shales.

isotherm data are given in Table S5 in the Supporting Information. Nitrogen uptakes on Harderode shales were too low to allow measurements of isotherms. This is in contrast to the CO_2 isotherms for the Harderode shales at −78 °C, which, although having the lowest uptake, have isotherm shapes consistent with the other samples. This difference in isotherm uptake is attributed to activated diffusion effects for N_2 in ultramicroporosity at −196 °C, which is not apparent for CO_2 adsorption at −78 °C.[50,51] The shapes of the N_2 adsorption isotherms indicate micropore filling (up to $p/p_0 \approx 0.2$) and gradual increase for $p/p_0 > 0.2$ and increased upward isotherm curvature close to $p/p_0 = 1$. Maximum uptakes at $p/p_0 \approx 1$ were in the range of 0.22−0.59 mmol g^{-1} on shale and 0.32−4.0 mmol g^{-1} on kerogen (see Table S5 in the Supporting Information). Steep uptake of nitrogen isotherms of Hadessen shales and kerogens at −196 °C at very low p/p_0 ($p/p_0 < 0.02$) indicates the filling of ultramicropores.[52]

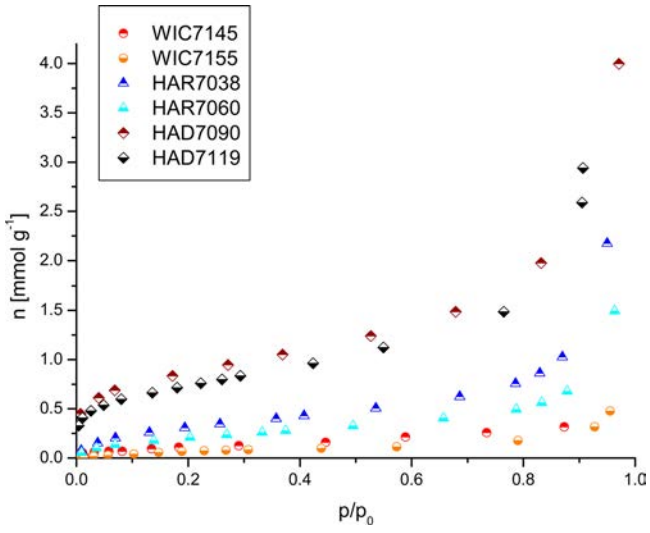

Figure 5. N_2 adsorption isotherms at −196 °C for Posidonia kerogens.

Surface areas calculated from the BET isotherms are given in Table 4. Since some activated diffusion effects were observed for N_2 adsorption on HAR shales and kerogens at −196 °C, the surface areas were not suitable for comparisons between samples.

3.2.3. Micropore Volumes. Some authors favor the use of carbon dioxide adsorption at 0 °C for the characterization of the microporous structure in activated carbons and coals, because, compared with N_2 at −196 °C, the higher temperature for CO_2 adsorption overcomes kinetic limitations due to activated diffusion.[50,53,54] Carbon dioxide isotherms at 0 °C of shale and kerogen are Type I Isotherms (see Table S3 in the Supporting Information for tabulated data). Under these temperature and pressure conditions (<0.1 MPa), CO_2 sorption is limited to ultramicropores (less than ∼0.7 nm).[50,55] Maximum uptakes at $p/p_0 \approx 0.029$ were between 0.06 and 0.12 mmol g^{-1} for shales and between 0.27 and 0.74 mmol g^{-1} for kerogens (Table S3 in the Supporting Information). Thus, CO_2 uptake on kerogen is ∼5 times higher than on shales under these conditions.

The Dubinin−Radushkevich (DR) model was used to calculate ultramicropore volumes, using a density of 1.032 g cm^{-3} (liquid density of CO_2 at −20 °C).[56] A value of 1.023 g cm^{-3} was used previously in a detailed study of the adsorption of CO_2 on activated carbons.[50] In addition, a nonlocal density functional theory (NLDFT) equilibrium model with a kernel based on slit-shaped pores in carbon was used to calculate pore size distributions (see Supporting Information (Section G, Figures S7 and S8)) and micropore volumes from the isotherms. These pore size distributions (<5 nm) are shifted to slightly lower pore sizes compared with Eagle Ford shale obtained from nitrogen (−196 °C).[57] Table 4 shows that the ultramicropore volume ranges in shales, estimated from the DR and NLDFT models were 4.6−8.0 mm^3 g^{-1} and 4.0−7.7 mm^3 g^{-1}, respectively. Ultramicropores thus represent ∼12% of total pore volume in Wickensen and Hadessen samples, and 2% and 41% of total pore volume in the Harderode samples. Ultramicropore volumes follow the same trends as CO_2 sorption pore volumes. There is only a weak trend of micropore volume with maturity for the shales.

Ultramicropore volumes in kerogens are much higher than in shales, ranging from 27.0 to 54.6 mm^3 g^{-1}, estimated from the

dx.doi.org/10.1021/ef402466m | Energy Fuels 2014, 28, 2886−2901

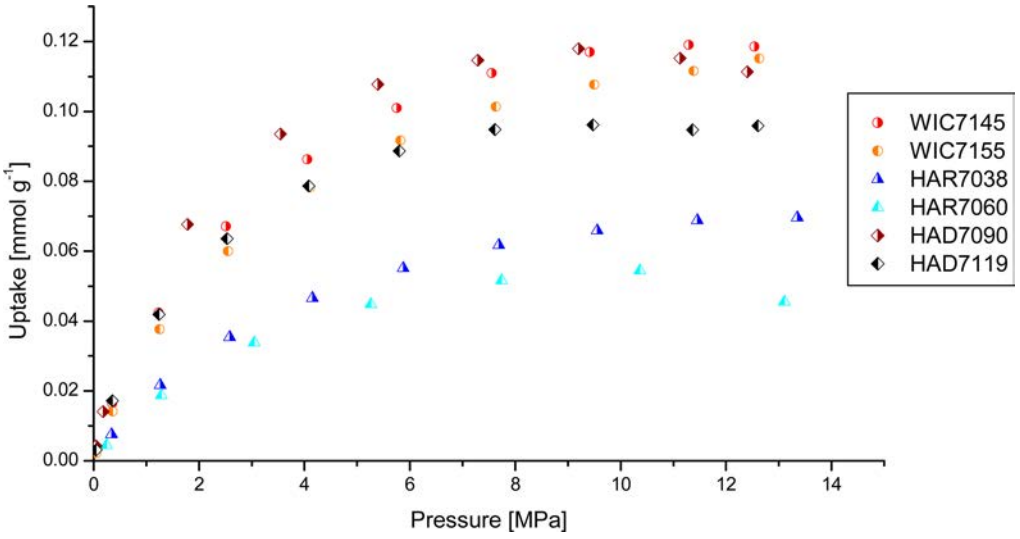

Figure 6. Methane surface excess adsorption isotherms at 45 °C on Posidonia shales.

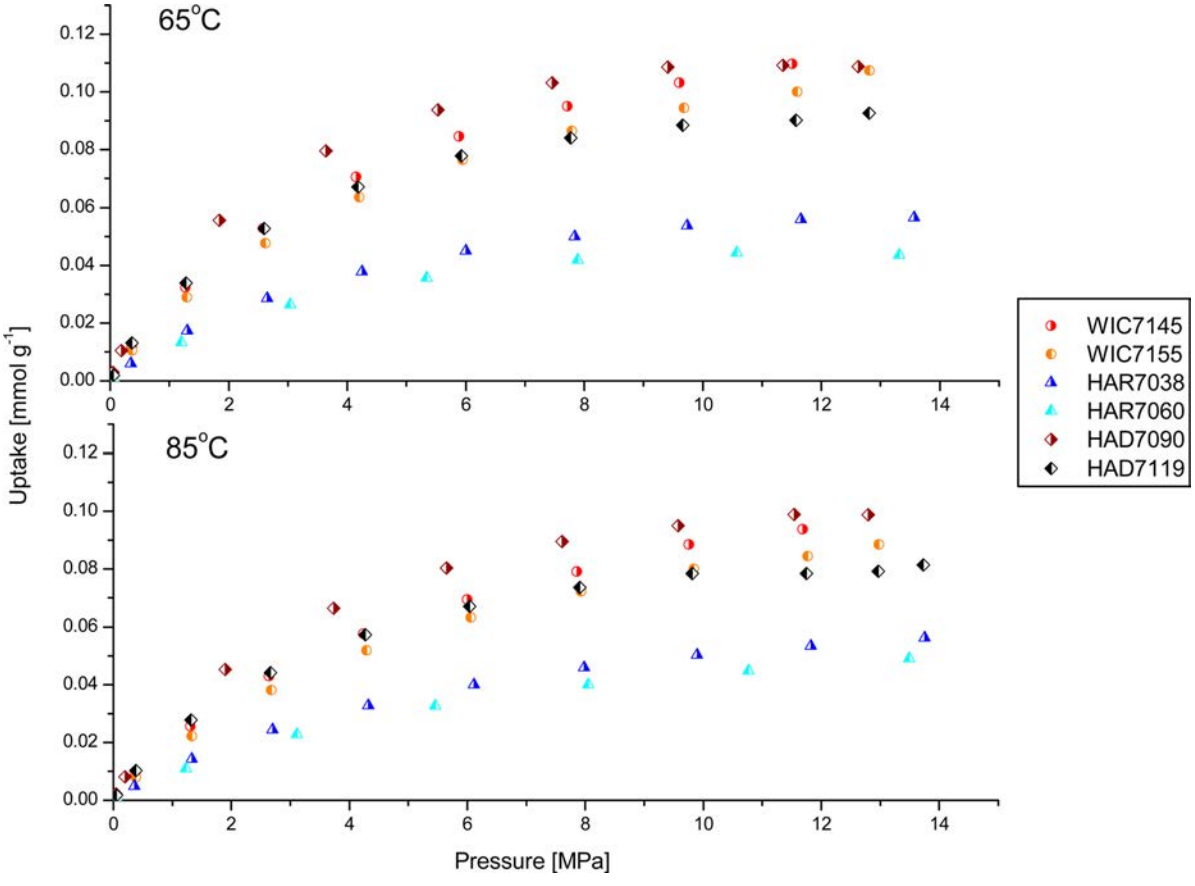

Figure 7. Methane surface excess adsorption isotherms at 65 and 85 °C on Posidonia shales.

DR model, and 21.8 to 50.8 $mm^3\ g^{-1}$ according to the NLDFT model (see Table 4). Ultramicropore volumes are similar in Wickensen (R_0 = 0.53%) and Harderode (R_0 = 0.89%) samples, but are almost double in the Hadessen (R_0 = 1.45%) samples (see Table 4).

Even though the models are entirely different, NDLFT micropore volumes generally agree well with the DR ultramicropore volumes. NDLFT micropore size distributions are shown in the Supporting Information (Figures S7 and S8). The pore size distribution show very little porosity above a pore width of ~1 nm, confirming that CO_2 at 0 °C and 0.1 MPa is limited to ultramicroporosity.

DR micropore volumes were also calculated from −196 °C nitrogen isotherms. At low relative pressure, nitrogen fills micropores <2 nm providing there is no activated diffusion or molecular sieving. The N_2 micropore volumes are shown in Table 4. For kerogen, the N_2 micropore volumes are significantly lower than the CO_2 ultramicropore volume, probably reflecting some activated diffusion or molecular sieving, as mentioned in section 3.2.2. However, the nitrogen

dx.doi.org/10.1021/ef402466m | Energy Fuels 2014, 28, 2886−2901

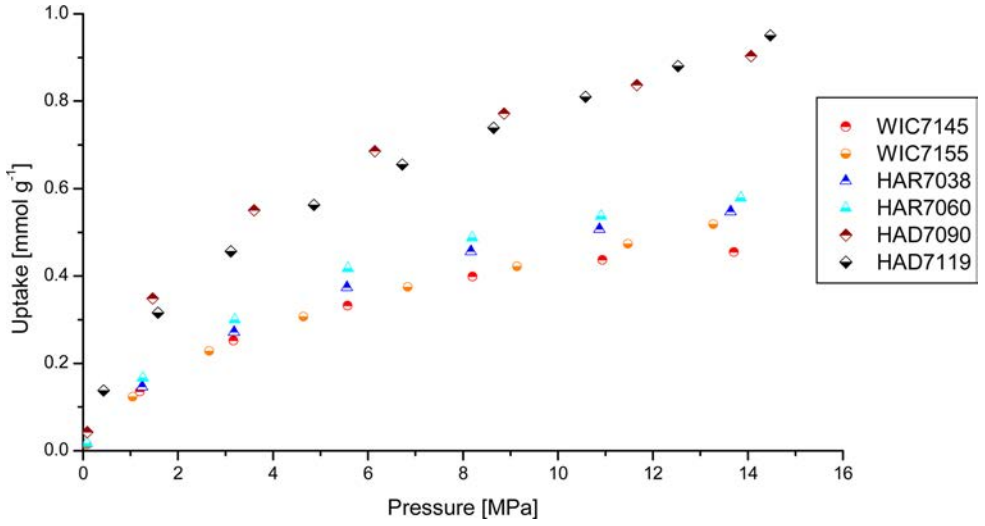

Figure 8. Methane surface excess isotherms for Posidonia kerogens at 45 °C.

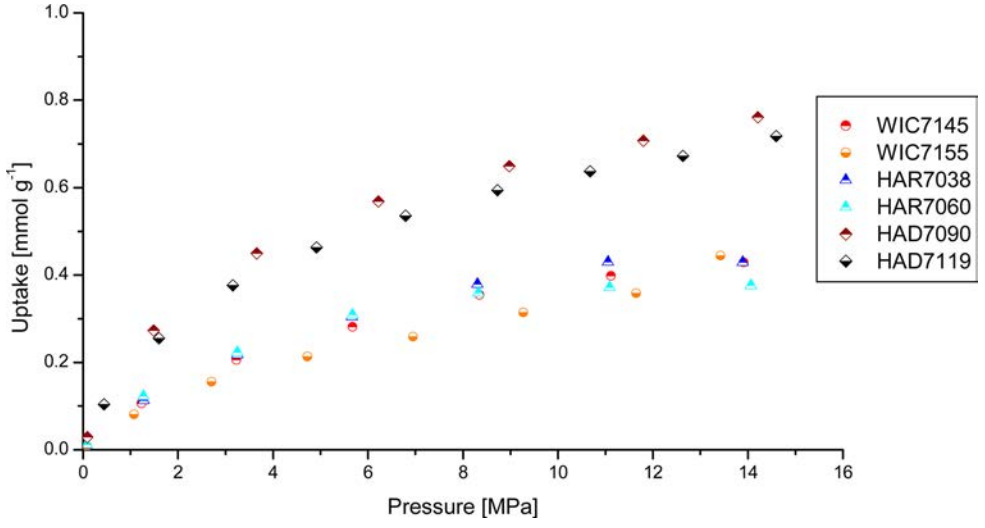

Figure 9. Methane surface excess adsorption isotherms for Posidonia kerogens at 65 °C.

micropore volumes increase with increasing maturity in a similar manner to the CO_2 ultramicropore volumes. This large increase in micropore volume might be due to the generation of slightly larger micropores in kerogen, through which nitrogen can diffuse more readily.

3.3. Methane Sorption. *3.3.1. Shale.* Shale isotherms were measured at 45, 65, and 85 °C and up to ∼14 MPa. Excess shale isotherms are shown in Figures 6 and 7. Tabulated isotherm data are given in the Supporting Information (Table S6). Isotherms at 45 °C for HAR7060 and HAD7090 show a distinct excess maximum, while the other isotherms show plateaus. Maximum surface excess uptakes are between 0.096 mmol g^{-1} and 0.119 mmol g^{-1} for Wickensen and Hadessen shales, while uptake on Harderode shales were lower, with maxima of 0.054 mmol g^{-1} and 0.070 mmol g^{-1} (see Table S6 in the Supporting Information). Maximum methane surface excess uptake decreases with increasing temperature for all shales. Furthermore, at 65 and 85 °C, the isotherms do not have a distinct maximum in the pressure range used in this study.

3.3.2. Kerogen. Kerogen isotherms were measured at 45 and 65 °C and up to ∼14 MPa. The surface excess isotherms are shown in Figures 8 and 9, and tabulated data are given in Table S6 in the Supporting Information. The pressure range is not large enough for the isotherms to reach the excess maximum or plateau. WIC and HAR kerogens take up between 0.45−0.58 mmol g^{-1} at ∼13.5 MPa and 45 °C, which is similar to Pennsylvanian coals of various rank (V_R = 0.72%−1.56%).[58] Maximum uptake on HAD kerogens (R_0 = 1.45%) was higher (0.90−0.95 mmol g^{-1} at 45 °C and ∼14 MPa) than on WIC (R_0 = 0.53%) and HAR (R_0 = 0.89%) kerogens. This shows the increase in adsorption capacity at the onset of the gas-window.

3.3.3. Methane Sorption and Pore Volumes. There is only a weak correlation (R^2 = 0.48) of maximum excess uptake at 45 °C on shale and TOC (see Figure 10). However, there is a very strong correlation of methane uptake and CO_2 sorption pore volume. Figure 11 shows methane uptake on shale and kerogen at 45 °C and 10.0 MPa against the CO_2 sorption pore volume, with a regression line that goes through the origin. A strong correlation also exists between methane uptake at 65 °C and 11.5 MPa and CO_2 sorption pore volume (see Figure 12). Similar correlations are obtained at lower pressures (see Figures S9a and S9b in the Supporting Information) and also at 85 °C (see Figure S9c in the Supporting Information). The

dx.doi.org/10.1021/ef402466m | Energy Fuels 2014, 28, 2886−2901

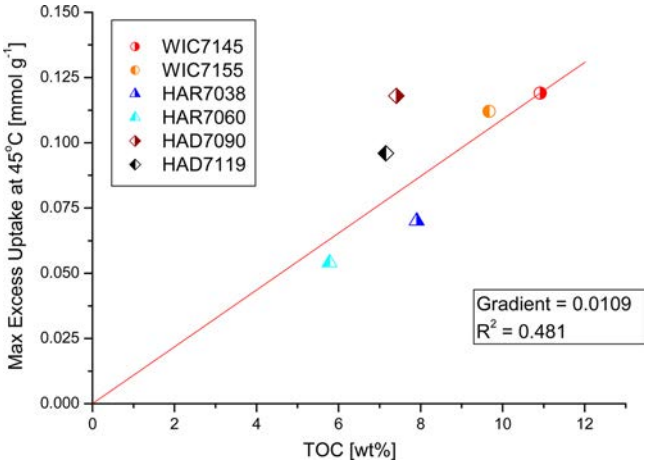

Figure 10. Plot of maximum methane surface excess uptake at 45 °C versus TOC.

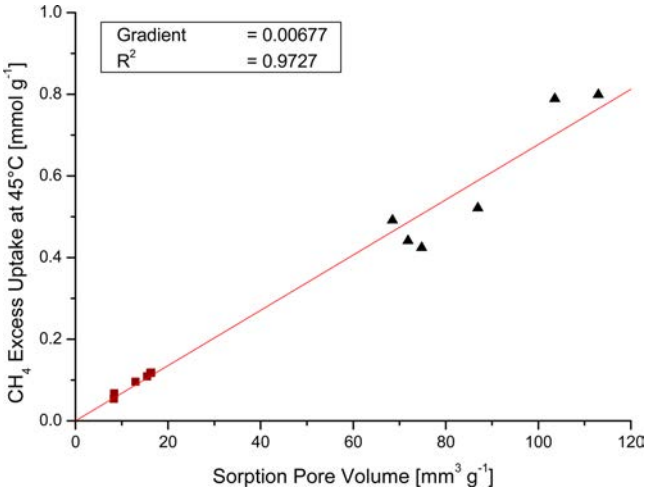

Figure 11. Graph of CH_4 maximum excess uptake at 45 °C and 10 MPa on shale (squares, ■) and kerogen (triangles, ▲) versus CO_2 sorption pore volume (−78 °C).

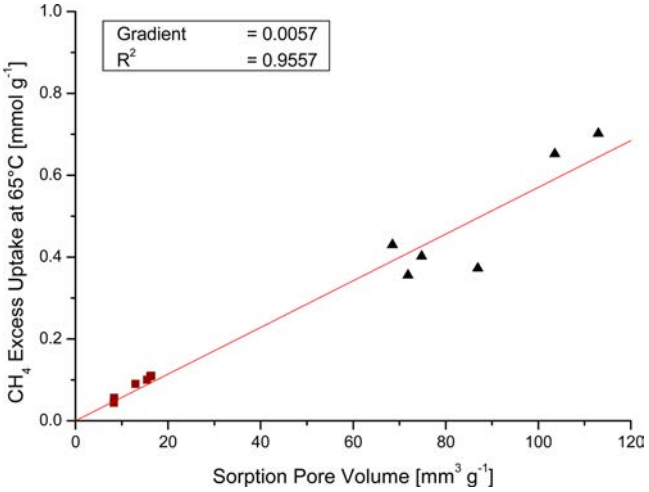

Figure 12. Graph of CH_4 excess uptake at 65 °C and 11.5 MPa on shale (squares, ■) and kerogen (triangles, ▲) versus CO_2 sorption pore volume (−78 °C).

correlations suggest that supercritical methane sorption on Posidonia shales and kerogens takes mainly place in pore volumes as measured by CO_2 sorption at −78 °C. Both the CO_2 subcritical and methane supercritical adsorption studies show that kerogens have much larger adsorption than for the corresponding shales (see Figures 11 and 12). Comparison of kerogen and shale isotherms with TOC measurements indicate that the shale adsorption exceeds that which can be taken into account by the kerogen alone, indicating that significant adsorption occurs in the inorganic phase of the shale. The sorption mass balances for kerogens and inorganic phase materials (clays, etc.) are discussed later.

3.3.4. Absolute Isotherms and Parametrization. The absolute isotherm can be calculated from the excess isotherm using the following equation:

$$n_{ab} = n_{ex} + \rho_b V_{ad} \quad (1)$$

where n_{ex} is the excess amount adsorbed, ρ_b the bulk gas-phase density, and V_{ad} is the adsorption pore volume. Equation 1 has been used for crystalline zeolites and metal organic frameworks, where the structure can be determined from XRD or neutron diffraction studies. Good agreement has been observed between crystallographic data and pore volumes measured by gas adsorption for microporous metal organic framework materials.[59,60] In these materials, V_{ad} is assumed to be equal to the crystallographic pore volume, which is an inherent property of the adsorbent.[61,62] However, for heterogeneous materials, such as shales, which have a wide pore size distribution, this is more problematic, since adsorption in the larger pores may not be significant.[63] In the shales used in this study, the subcritical CO_2 sorption pore volumes were 21%−32% of the total pore volume for the WIC and HAD shale samples and 46%−66% of the total pore volume for the HAR shale samples (see Table 4). It is evident that in these materials, V_{ad} is significantly lower than the total pore volume. It is important to distinguish between the adsorbed and bulk gas phases in shale in order to understand the occurrence of adsorbed gas in shale; therefore, V_{ad} must be estimated. Studies of a high-maturity Alum shale showed that subcritical pore volumes obtained from adsorption of CO_2 (−78 and 0 °C), N_2 (−196 °C), and CH_4 (−161 °C) agreed within ±5%.[11] Hence, the CO_2 sorption pore volume at −78 °C is a reasonable estimate for an upper limit for V_{ad}. Therefore, in this study, a sorption volume balance for the shales was investigated by measuring the total pore volume (<1093 nm) from helium pycnometry, grain density, and mercury bulk density; from mercury injection capillary pressure porosimetry; and from gas sorption pore volumes.

The Washburn equation indicates that mercury enters pores with constrictions with equivalent diameters >1093 nm at 1.379 MPa. Therefore, at 1.379 MPa, $1/\rho_{Hg\ Bulk}$ will be equal to the volume of the shale and pores <1093 nm, where $\rho_{Hg\ Bulk}$ is the mercury bulk density of the shale. Assuming helium enters all accessible pores and is not adsorbed; $1/\rho_{He}$ is equal to the volume of shale, where ρ_{He} is the density of the shale measured by helium pycnometry. Therefore, the total pore volume (<1093 nm) is given by the equation

$$\text{Total pore volume (<1093 nm)} = \frac{1}{\rho_{Hg\,Bulk}} - \frac{1}{\rho_{He}} \quad (2)$$

and the total porosity (<1093 nm) is given by the equation

$$\text{Total porosity (1093 nm)} = 1 - \frac{\rho_{Hg\,Bulk}}{\rho_{He}} \quad (3)$$

dx.doi.org/10.1021/ef402466m | Energy Fuels 2014, 28, 2886−2901

Alternatively, since the helium and grain densities are similar within experimental error, ρ_{He} can be replaced by ρ_{Grain} in eqs 2 and 3.

Figure 3 shows that a graph of total pore volume (<1093 nm) versus CO_2 sorption pore volume (CO_2 SPV) + mercury injection pore volume ($MICP_{PV}$) corresponding to eq 4 below, has good linearity (R^2 = 0.974) for the six shales studied, which vary markedly in maturity.

$$\text{Total pore volume } (<1093 \text{ nm}) = CO_2 \text{ SPV} + \text{MICP}_{PV} \quad (4)$$

The $MICP_{PV}$ corresponds to the difference between the mercury injected at 1.379 and 268.9 MPa, and CO_2 SPV is the pore volume obtained from CO_2 adsorption at 0.1 MPa and −78 °C using a CO_2 adsorbed phase density of 1.177 g cm^{-3}. The CO_2 SPV characterizes the microporosity and some mesoporosity where gas adsorption predominates, while the $MICP_{PV}$ characterizes the mesoporosity >5.6 nm and macroporosity up to 1093 nm. The upper size limit for significant CO_2 adsorption is unknown, but the linear relationship in Figure 3 indicates that it is ∼5−6 nm. However, there will be very small amounts of adsorption in larger pores. The linearity of the relationship indicates that all the accessible porosity <1093 nm has been taken into account by the combination of CO_2 sorption and mercury injection. It is not possible to use mercury injection porosimetry for isolated kerogens. The strong linear (R^2 = 0.9557 and 0.9727) correlation between CH_4 sorption uptake and CO_2 sorption pore volume for both shales and kerogens used in this study suggest that supercritical methane sorption in shales and kerogen takes place in the CO_2 sorption pore volume (see Figures 11 and 12). These correlations support the use of the CO_2 sorption pore volume (−78 °C) for V_{ad} to estimate absolute isotherms and, thus, quantify the sorbed phases in shales. Also, it provides an estimate of adsorbed phase versus bulk "free" gas phase contributions to methane stored in shale.

The absolute isotherms of shales and kerogen are shown in Figures 13 and 14. Absolute amounts on HAD shales at ∼13 MPa and 85 °C are 0.14 and 0.18 mmol g^{-1}. HAD kerogens exhibit much higher absolute amounts adsorbed of 1.21 and 1.31 mmol g^{-1} (at 13 MPa and 65 °C). Mass balance calculations between the shale and kerogen data obtained by

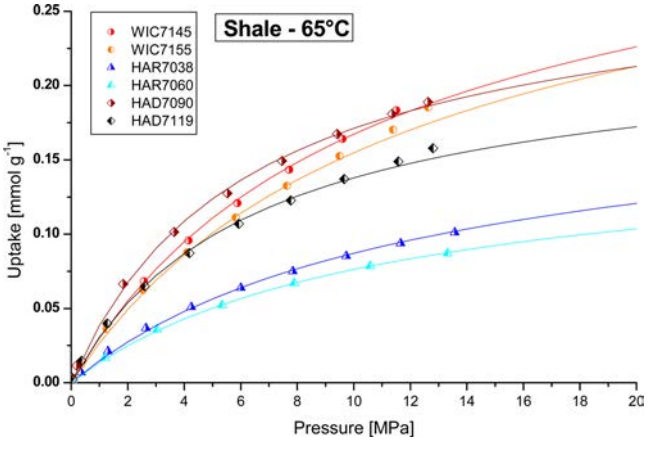

Figure 13. Absolute methane isotherms on shale at 65 °C. It is assumed that the volume of the adsorbed phase is equal to the CO_2 sorption pore volume. The lines represent the Langmuir fit to the absolute and excess data (simultaneous fit).

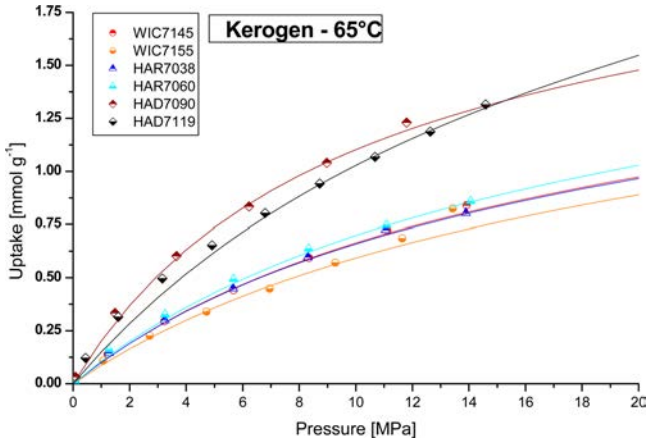

Figure 14. Absolute methane isotherms on kerogen at 65 °C. It is assumed that the volume of the adsorbed phase is equal to the CO_2 sorption pore volume. The lines represent the Langmuir fit to the absolute and excess data (simultaneous fit).

normalizing these uptakes with TOC and comparison with the uptake on shale under the same conditions, shows that ∼50% of the methane uptake in HAD shales is within the kerogen.

The DR and Langmuir equations can be used as semi-empirical equations to parametrize the methane absolute isotherms. The supercritical DR equation has been shown to describe methane isotherms more accurately than the Langmuir equation over a wide temperature range (27−200 °C) for an Alum shale sample.[11] The DR micropore volume was 77% of the CO_2 sorption pore volume in the Alum shale, and this is significantly higher than the shales used in this study, which were in the range of 40%−62%. However, the Posidonia shale and kerogen absolute and excess isotherms for 45, 65, and 85 °C were described more accurately by a modified version of the Langmuir equation:

$$n_{ab} = n_{ab,max}\frac{K(T)f}{1 + K(T)f} \quad (5)$$

where $n_{ab,max}$ is the maximum absolute amount adsorbed, $K(T)$ is the Langmuir parameter, and f is the fugacity. One fitting parameter can be eliminated by using $n_{ab,max}$ = CO_2 SPV × $\rho_{ad,max}$, where CO_2 SPV is the CO_2 sorption pore volume and $\rho_{ad,max}$ is the maximum adsorbed phase density.

The shale and kerogen absolute and excess isotherms were fitted to eq 5 with two fitting parameters for shales and kerogens, the temperature-dependent Langmuir parameter $K(T)$ and the maximum adsorbed phase density ($\rho_{ad,max}$). Because of the narrow temperature range (45−85 °C for shale and 45−65 °C for kerogen) $\rho_{ad,max}$ was assumed to be independent of temperature. Other studies on shale sorption have used pressure instead of fugacity in the Langmuir model.[12,16] The use of pressure instead of fugacity gave almost identical results to those presented in Table 4.

Good fits were obtained for shale and kerogen isotherms. The calculated parameters are shown in Table 5 and the fits of the model to the absolute isotherms at 65 °C are shown in Figure 13 for shale and Figure 14 for kerogen. The corresponding CH_4 adsorption data at 45 and 85 °C are given in the Supporting Information (Figures S4−S6). The adsorbed phase densities of methane on shale are all below the liquid density of methane (425.1 kg m^{-3} at the boiling point: −161.49 °C and 101.3 kPa).[56] The hypothesis is that adsorbed

dx.doi.org/10.1021/ef402466m | Energy Fuels 2014, 28, 2886−2901

Table 5. Parameters Calculated by Fitting the Langmuir Equation to the Shale Methane Sorption Data[a]

	Shale					Kerogen			
sample	ρ_{ad} [kg m^{-3}]	$K(45)$ [MPa^{-1}]	$K(65)$ [MPa^{-1}]	$K(85)$ [MPa^{-1}]	error	ρ_{ad} [kg m^{-3}]	$K(45)$ [MPa^{-1}]	$K(65)$ [MPa^{-1}]	error
WIC7145	371	0.112	0.087	0.068	1.3×10^{-4}	478	0.058	0.048	2.0×10^{-3}
WIC7155	388	0.099	0.077	0.061	8.5×10^{-5}	503	0.057	0.040	2.7×10^{-3}
HAR7038	415	0.102	0.074		3.2×10^{-5}	516	0.064	0.048	2.0×10^{-3}
HAR7060	340	0.115	0.084		4.7×10^{-6}	441	0.069	0.047	4.5×10^{-3}
HAD7090	293	0.193	0.152	0.118	1.5×10^{-4}	356	0.118	0.089	9.6×10^{-3}
HAD7119	299	0.188	0.147	0.114	8.1×10^{-5}	614	0.054	0.040	4.5×10^{-2}

[a]The error column shows the accumulated error (residuals sum of squares) of the fit. The adsorbed phase density is assumed to be constant over the (relatively small) temperature range.

phase densities in the pores do not exceed the liquid density of the sorptive. The adsorbed phase densities of WIC and HAR shales are within 11% of the methane adsorbed phase density on shale determined by molecular simulations (370 kg m^{-3}) by Ambrose et al.[64] The adsorbed phase densities of HAD shales (~290 kg m^{-3}) are lower. This could be due to wider pores in the HAD gas-window shales (R_0 = 1.45%), as indicated earlier. The Langmuir constants and adsorbed phase densities are similar to the values determined by Gasparik et al. on Aalburg and Sleen shale samples at 65 °C ($K(65)$ = 0.064−0.104 MPa^{-1}; 295−332 kg m^{-3}).[16] The calculated adsorbed phase densities for all kerogens with the exception of HAD7090 are above the liquid methane density, suggesting that the Langmuir model may have significant limitations for determining physically reasonable sorption parameters or possibly, there are sorption induced volumetric changes.

3.3.5. Distribution of High-Pressure Methane Sorption. Mass balances of methane sorption on shales were determined to investigate the distribution of sorption sites between kerogen plus clay minerals and the organic−inorganic interface. Methane sorption on clay minerals has been studied previously.[65,66] Ji et al.[65] measured methane sorption at 65 °C up to ~10 MPa on montmorillonite, kaolinite, chlorite, and illite at 65 °C, while Liu et al.[66] measured methane sorption on montmorillonite, kaolinite, and illite at 60 °C and up to 18 MPa. The clay sorption data and kerogen sorption data were normalized by the XRD data and TOC, respectively, and compared against the shale isotherm at 65 °C. Results are shown in Figure 15. Approximately 45%−60% and 60%−70% of the methane sorption can be attributed to clays and kerogen in WIC and HAD shales, respectively, whereas kerogen and clay minerals can account for the entire sorption capacity measured on HAR shales.

3.3.6. Enthalpy of Adsorption of Shales. The isosteric enthalpies of adsorption can be calculated for a pure gas, using the equation below:[67]

$$Q_{st,n} = RT^2\left[\frac{\delta \ln P}{\delta T}\right]_n \tag{6}$$

where $Q_{st,n}$ is the isosteric enthalpy of adsorption at a surface excess loading n, P is the pressure, T the temperature, and R the gas constant. The surface excess is approximately equal to the absolute amount adsorbed at low pressure. The isosteric enthalpy of adsorption at zero surface coverage ($Q_{st,n=0}$) is a fundamental measure of the adsorbate interaction with the adsorbent. At the zero surface coverage adsorption limit, the isosteric enthalpies of adsorption derived from surface excess and absolute isotherms should be identical.

The methane absolute isotherms were calculated using eq 1 and the CO_2 sorption pore volume (−78 °C). The isosteric enthalpies of adsorption of methane on shale and kerogen were calculated at zero surface coverage by two methods (Myers and Monson[68] and virial equation[69,70]). The virial equation at low surface coverage is given below:

$$\ln\left(\frac{n_{ab}}{P}\right) = A_0 + A_1 n_{ab} \tag{7}$$

where n_{ab} is the absolute amount adsorbed (mmol g^{-1}), p is the pressure (Pa), and A_0 and A_1 are virial parameters. The slope of the graph of A_0 against T^{-1} gives ($Q_{st,n=0}/R$). The Henry's law constant is given by the equation below:

$$K_H = \exp(A_0) \tag{8}$$

The $Q_{st,n=0}$ was also determined using the Langmuir equation (eq 5), which provided a good fit for the experimental data. Myers and Monson defined the absolute uptake as the amount of gas inside the pore volume and used the Langmuir equation to derive Q_{st}.[68] In the case of shales, which have a significant amount of mesoporosity and macroporosity, the sorption pore volume is the volume of increased density, because of sorption. The equation derived is

$$C = \frac{1}{P^\circ}\exp\left(\frac{A}{R}\right)\exp\left(\frac{-B}{RT}\right) \tag{9}$$

where C is the constant in the Langmuir equation, which is a function of temperature; B is the enthalpy of adsorption (kJ mol^{-1}), and P° = 1 bar is the pressure at the perfect-gas reference state. The temperature-independent component $\exp(A/R)$ is an entropic factor.

The enthalpies of CH_4 adsorption at zero surface coverage on shales and kerogens calculated by both methods are shown in Table 6. The enthalpies of adsorption for shales and kerogen are very similar for calculations by both methods. The average values for $Q_{st,n=0}$ for shale are 14.4 ± 1.6 kJ mol^{-1} (via the virial method[69]) and 12.2 ± 1.0 kJ mol^{-1} (via the Myers and Monson method[68]), while the values for kerogens are 13.1 ± 1.9 kJ mol^{-1} (via the virial method[69]) and 13.4 ± 3.0 kJ mol^{-1} (via the Myers and Monson method[68]). No clear trend with maturity was observed. The $Q_{st,n=0}$ values are slightly lower than the corresponding enthalpy of 19.2 ± 0.1 kJ mol^{-1} determined at 0.025 mmol g^{-1} for an Alum shale, which had a greater proportion of ultramicroporosity. Similar results have been obtained for a Barnett shale from the gas-window (R_0 = 2.01%, Q_{st} = 18.4 kJ mol^{-1}).[12] Shales from the pre-gas-window had lower isosteric enthalpies of adsorption (Q_{st} = 7.3−15.3 kJ mol^{-1}).[12] The range of isosteric enthalpies obtained for CH_4 adsorption on other porous materials are similar (activated

dx.doi.org/10.1021/ef402466m | Energy Fuels 2014, 28, 2886−2901

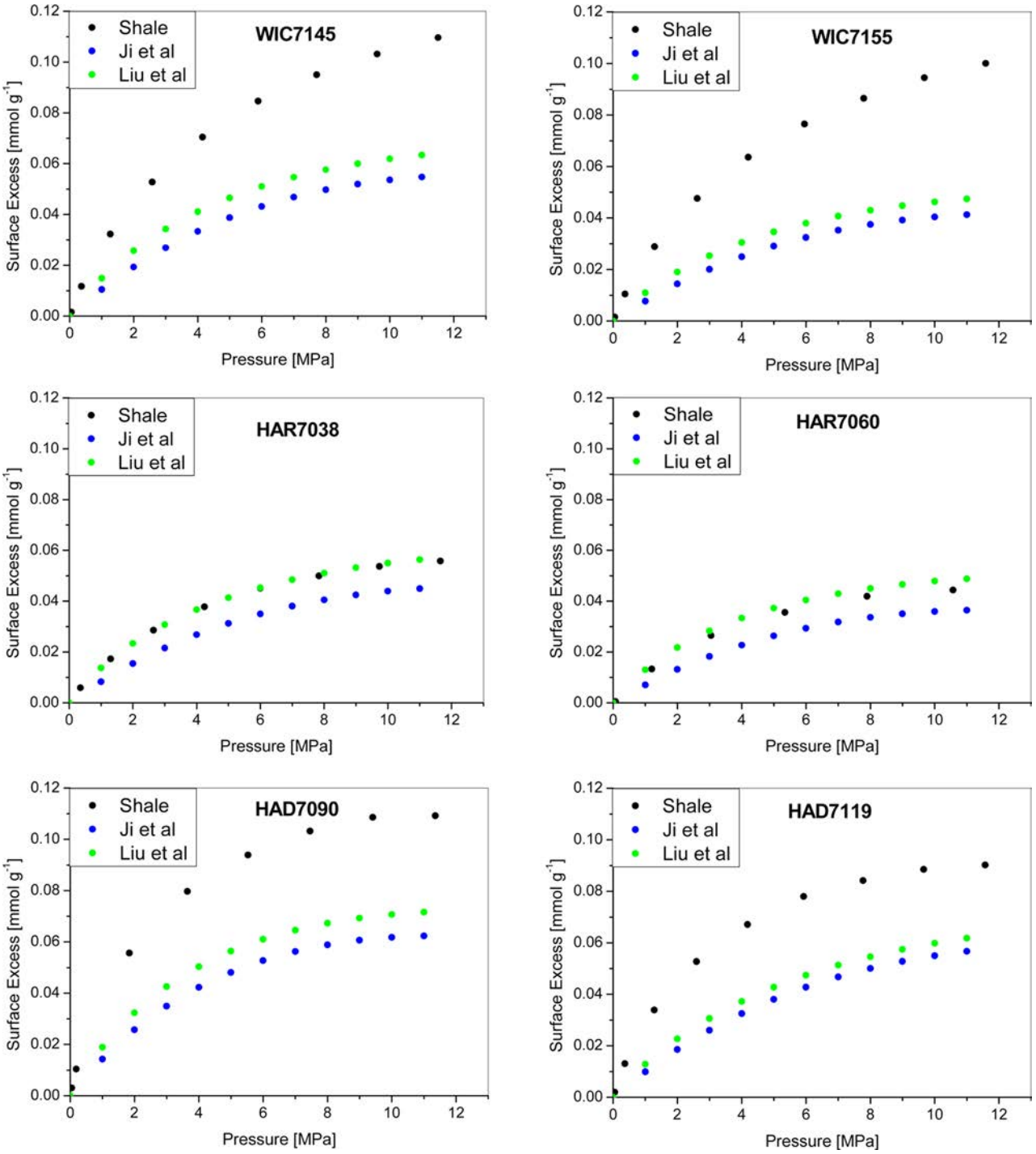

Figure 15. Mass balances of methane surface excess sorption on shale at 65 °C. The experimental shale excess isotherms (black) are compared to mass balance isotherms calculated from the sorption excess data for kerogen, TOC, and mineral composition determined in this study and sorption data for clay minerals reported by Ji et al.[65] (blue) and Liu et al.[66] (green). The isotherms were obtained by fitting kerogen and clay mineral data to the Langmuir equation, and components were normalized and summed for comparisons with the experimental shale isotherms.

carbon (Q_{st} = 9−20 kJ mol^{-1})[71−73] and coal (Q_{st} = 10−22 kJ mol^{-1})[74,75]). It is apparent that the strength of interactions of methane with porosity in various shales are similar and also, similar to CH_4 adsorption on carbonaceous materials. There are, at most, small differences in adsorption enthalpy with maturity or uptake for the samples studied. The thermodynamics discussed above and the correlation of supercritical CH_4 adsorption uptake with CO_2 sorption pore volume (−78 °C) for shales suggest that the amount adsorbed is controlled by the available porosity (less than ~6 nm) rather than the strength of the interaction of CH_4 with the pore walls in shales.

4. DISCUSSION

Comparison of the subcritical CO_2 isotherms for Posidonia shales and the corresponding kerogen isotherms shows that they have similar shapes. Both the DR micropore volumes (CO_2, 0 °C) and sorption pore volumes (CO_2, −78 °C) increase with increasing total pore volumes and have

dx.doi.org/10.1021/ef402466m | Energy Fuels 2014, 28, 2886−2901

Table 6. Isosteric Enthalpies of Adsorption of CH_4 on Shales and Kerogens at Zero Surface Coverage ($Q_{st,n=0}$)

	$Q_{st,n=0}$ (kJ mol^{-1})					
calculation method[a]	WIC7145	WIC7155	HAR7038	HAR7060	HAD7090	HAD7119
Shale						
virial equation	15.1 ± 0.1	15.7 ± 2.8	11.8 ± 0.4	12.9 ± 2.4	15.7 ± 0.8	15.4 ± 0.1
Myers and Monson[68]	11.7 ± 0.1	11.2 ± 0.4	14.0 ± 0.5	12.7 ± 1.9	11.7 ± 0.1	12.1 ± 0.3
Kerogen						
virial equation	11.2	*b*	14.5	12.8	15.7	11.5
Myers and Monson[68]	8.5 ± 1.3	15.8 ± 2.8	12.9	17.2 ± 1.4	12.6 ± 1.7	13.4 ± 0.8

[a]The virial equation was used to calculate the enthalpy at zero surface coverage (ZSC) $Q_{st,n=0}$ from the absolute isotherm. The method of Myers and Monson was used to calculate $Q_{st,n=0}$. [b]For the kerogen WIC7155 sample, the sorption data did not give a suitable fit to the virial equation.

approximately linear trends for the shales (see Figures S11a, S11b, and S11c in the Supporting Information). The DR micropore volumes (CO_2, 0 °C) and sorption pore volumes (CO_2, −78 °C) has a similar trend for the kerogens and better linearity (R^2 = 0.8893) (see Figure S11d in the Supporting Information). However, no specific trends are expected between these parameters. The DR micropore volumes (CO_2, 0 °C) and sorption pore volumes (CO_2, −78 °C) for the kerogens are 3.6−9.1 and 4.6−10.5 times larger than the corresponding shales indicating the potential importance of the kerogen in determining CH_4 storage capacity. Comparison of the DR micropore volumes (CO_2, 0 °C) and sorption pore volumes (CO_2, −78 °C) for shales and kerogens shows no correlation suggesting that adsorption in the inorganic phase (clays, etc.) makes a significant contribution to subcritical adsorption (see Figures S11e and S11f in the Supporting Information). Comparison of the supercritical high-pressure methane isotherms for the Posidonia kerogens and shales shows that similar trends to the CO_2 subcritical isotherms are observed, with the kerogen uptakes being ∼3.6−8.4 times greater than the corresponding shale at 11.5 MPa and 65 °C. However, the TOC values for the samples studied are in the range of 5.78%−10.92%; therefore, the inorganic phase comprises >89% of the shales. The sorption mass balance between kerogen and shale indicates that methane storage in the inorganic phase of dry shales is also significant.

Posidonia kerogens have DR micropore volumes that are at the lower end of the range of micropore volumes measured on various coals (0.014−0.057 cm^3 g^{-1}).[76−78] A trend of DR micropore volume with maturity for coals has been reported with the DR micropore volume decreasing from high-volatile bituminous coals to medium-volatile bituminous coals and then increasing with further coalification.[45,76,79] The decrease in micropore volumes was attributed to the filling of pores by low-volatile hydrocarbons and the subsequent increase to the cracking of the occluded oils with coalification.[45,79] Similar trends were observed in DR micropore and sorption pore volumes in this study, suggesting that there is pore generation and/or pore opening by cracking of occluded oil in gas-window Posidonia kerogens. Micropore "blocking" by bitumen in the oil-window kerogens (HAR) may occur, similar to that observed with coal. The presence of low-volatile bitumen is suggested by the relatively low helium densities of HAR kerogens, compared to those of HAD kerogens, which had the highest densities (see Table 1). The shale CO_2 DR micropore and sorption pore volumes reach a minimum in the oil-window. However, kerogens do not show a well-defined minimum in the oil-window. There is no significant change from WIC to HAR; however, an increase is observed when changing to HAD. It is apparent that changes in the microporosity of kerogen are probably controlling changes in the microporosity of shales into the gas-window.

The shale pore volume is composed of contributions from inorganic materials (including phyllosilicates, etc.), kerogens, and the interface region between these materials. The contribution of the kerogen component to the shale porosity can be determined by normalizing the kerogen pore volume with TOC. This shows that approximately half of the CO_2 sorption pore volume for a given shale is within the organic matter for all Posidonia shale samples. The other part of the porosity cannot be attributed to any specific mineral type, because comparisons of mineral composition with pore volumes do not show any correlations. However, previous publications have concluded that micropores are present in clay but not in quartz,[14] although the clay content variation in Posidonia shales (illite/smectite ranging from only 18.5−26.2 wt %, kaolinite 1.1−8.9 wt %) is too small to show any trend with pore volume. The role of clays for sorption in dry shales is consistent with the similar shapes of kerogen and clay mineral isotherms.[14]

Since the sum of porosity measured via (a) CO_2 adsorption at −78 °C and (b) mercury injection is very similar to total porosity, and since mercury injection measures pore constrictions larger than ∼6 nm, we infer that most of the CO_2 sorption porosity is in pores smaller than ∼6 nm. The very strong correlation between CH_4 maximum excess uptake and CO_2 sorption volume suggests that most CH_4 is sorbed in pores, which are smaller than ∼6 nm and associated with both kerogen and clay minerals. Grand Canonical Monte Carlo simulations of methane adsorption have been carried out for graphitic surfaces, as models for kerogens, across a range of pore sizes for various temperature and pressure conditions. The results suggest that adsorbed methane density changes nonmonotonically with increasing pore width, and decreases to a minimum in 1.2 nm pores at 12 MPa.[80] Cai et al.[81] suggested that the pore volume, with pore widths in the range 2−5 nm, was the primary control for methane adsorption capacity of coals from northeastern China.

Methane isotherms for shales and kerogens normalized to TOC are shown in Figure S10a−f in the Supporting Information. It is apparent that the TOC normalized isotherms for shales are always higher that the corresponding kerogen isotherms. This indicates significant methane adsorption in the inorganic component of the shale. A mass balance for CH_4 sorption based on the kerogen isotherms measured in this study and the illite or smectite isotherms published by Ji et al.[65] and Liu et al.[66] suggests that for HAR shales, all the CH_4 sorption can be explained by the uptake on clay minerals and kerogen. However, only 45%−60% of the sorption of WIC shales and 60%−70% of the sorption of HAD shales can be

explained by a mass balance of sorption by kerogen and clay minerals (Figure 15).[65,66] Sorption mass balances determined using kerogen and shale isotherms suggest that in dry natural shales, possibly significant sorption also occurs at interfaces between kerogen and clay minerals for the WIC and HAD shales. Also, the kerogen separation process may modify its adsorption characteristics, and some other inorganic materials that are not considered in the sorption mass balance may increase sorption.

We note that, since water is present in natural subsurface shales, pores associated with clay minerals may be at least partly water-filled, in which case they will not contribute to the sorption pore volume. The adsorbed phase in porous systems is in equilibrium with the homogeneous bulk gas phase in mesopores and macropores. Fracturing shale and releasing gas from the bulk gas phase allows the sorbed gas to desorb. The amount of gas released (sorbed + bulk gas) at reservoir temperatures can be estimated from the excess isotherms and total pore volumes. The amount of gas desorbed can be visualized directly from the absolute isotherms. Absolute CH_4 sorption on dry Posidonia shales at 65 °C and 15 MPa ranges from 0.092−0.202 mmol g^{-1} (66−144 scf t^{-1}) on dry shale, and from 0.76−1.32 mmol g^{-1} (540−942 scf t^{-1}) on dry kerogen. Absolute amounts adsorbed at 85 °C and 15 MPa are 103 and 127 scf t^{-1} in dry Hadessen shales. The shapes of the absolute shale and kerogen isotherms indicate that only small amounts of gas will desorb at high pressure. This is not only because most sorbed gas is within pores smaller than ∼6 nm, but also, comparison of the DR micropore volumes obtained from CO_2 adsorption at 0 °C suggests that 40%−62% of the sorption pore volumes in shales and 39%−53% in kerogen are ultramicroporous. Gas in ultramicropores is strongly sorbed because of the proximity of the walls and the resulting high sorption potential. Furthermore, there is no significant variation of enthalpies of adsorption determined from high-pressure methane isotherms, indicating that the interactions of the pore surfaces and the methane molecules are similar in all these Posidonia samples and is not affected by maturity.

Although N_2 isotherms at −196 °C are often used to characterize porosity, they can be misleading.[82] The narrowest ultramicroporosity cannot be accessed by nitrogen molecules at −196 °C, because of activated diffusion. Furthermore, microporous solids may give rise to unrealistically high BET surface areas as micropore filling may occur. Both issues have been pointed out on coal previously.[83]

While the supercritical DR equation produced good fits for CH_4 sorption in a previous study on Alum shale,[8] Posidonia shale are more accurately described by the Langmuir equation. In comparison to the Posidonia shales, the Alum shale has a larger proportion of ultramicroporosity (DR CO_2 ultramicropore volume = 12.9 mm^3 g^{-1}, CO_2 sorption pore volume = 16.8 mm^3 g^{-1}).[14] The DR model is based on micropore filling and, thus, it produced good results on ultramicroporous shales. The Posidonia shales have a much greater fraction of larger pores as shown by the ratio of the CO_2 (−78 °C) sorption pore volume to the CO_2 (0 °C) DR micropore volume (see Table 4), and this may be the reason for the Langmuir model providing a better fit than the DR equation for the Posidonia isotherm data.

5. CONCLUSIONS

Methane sorption capacities and pore characteristics of bulk shales and isolated kerogens have been determined for immature, oil-window, and gas-window samples from the Lower Toarcian Posidonia shale formation. Total porosities and CO_2 sorption volumes (−78 °C) of organic-rich Posidonia shales decrease through the oil-window and then increase into the gas-window. This implies that part of the sorption porosity is blocked by bitumen and then regenerated as a result of gas generation from bitumen and/or kerogen. Since (a) the sum of porosities measured by CO_2 at −78 °C and mercury injection are very similar to the corresponding total pore volume (<1093 nm) thereby accounting for all the available shale porosity and (b) mercury at 268.9 MPa occupies pores with constrictions larger than ca. 6 nm, we infer that porosity measured by CO_2 adsorption at −78 °C is largely within pores smaller than 6 nm. The CO_2 sorption pore volume represents 21%−66% of the total pore volume in these shales, with 10%−41% of the total pore volume in DR micropore pore (less than ∼0.7 nm) volume. Porosity information from subcritical nitrogen sorption at −196 °C is not applicable due to activated diffusion effects.

A modified Langmuir model including the sorption pore volume fits the absolute and surface excess CH_4 isotherms well and this provides a useful parametrization of the data. Methane is sorbed strongly in ultramicropores and will only be desorbed at low pressure. Enthalpies of methane adsorption on dry shales range from 11.2−15.7 kJ mol^{-1} and from 8.5−17.2 kJ mol^{-1} on kerogen, and are not related to maturity. The linear correlation between maximum CH_4 sorption and CO_2 sorption pore volume (−78 °C) is very strong for both shales and kerogens, and it suggests that the vast majority of sorbed CH_4 occurs in pores smaller than 6 nm, with approximately half of that within ultramicroporosity in the shales studied. Shale and kerogen mass balance considerations indicate that approximately half of the CH_4 sorption on dry shales takes place within the organic matter and this indicates the significance of the inorganic phase, including the role of clays and possibly the organic−inorganic interface as sorption sites in dry shales. However, caution is required in extrapolating these results to the subsurface, where water is present.

■ ASSOCIATED CONTENT

Supporting Information

Available Supporting Information includes the following: Kerogen isolation and verification of purity by X-ray diffraction (Figure S1), pyrite adsorption isotherms (Figure S2), CO_2 isotherms on shale at 0 °C (Figure S3), Langmuir parametrization data (Figures S4−S6), micropore size distributions (Figures S7 and S8), comparisons of various characterization parameters (Figures S9 and S11), kerogen pyrite content (Table S1), instrument parameters (Table S2), tabulated supercritical methane and subcritical carbon dioxide and nitrogen adsorption isotherm data (Tables S3−S6), and associated text. Kerogen isolation, are also included. Also, shale and kerogen isotherms, normalized to TOC, are compared in Figure S10. This material is available free of charge via the Internet at http://pubs.acs.org.

■ AUTHOR INFORMATION

Corresponding Author

*E-mail: mark.thomas@ncl.ac.uk.

Notes

The authors declare no competing financial interest.

■ ACKNOWLEDGMENTS

This work was supported by the Wolfson Foundation and the GASH project funded by Bayerngas, ExxonMobil, GdFSuez, Marathon, Repsol, Schlumberger, Statoil, Total, Vermilion, and Wintershall.

■ REFERENCES

(1) *U.S. Annual Energy Outlook 2013*; U.S. Energy Information Administration (EIA): Washington, DC, 2013.
(2) Borst, R. L. *Sedimentology* **1982**, *29*, 291.
(3) Yang, Y. L.; Aplin, A. C. *Mar. Pet. Geol.* **1998**, *15*, 163.
(4) Cartwright, J. A.; Dewhurst, D. N. *Geol. Soc. Am. Bull.* **1998**, *110*, 1242.
(5) Loucks, R. G.; Reed, R. M.; Ruppel, S. C.; Jarvie, D. M. *J. Sediment. Res.* **2009**, *79*, 848.
(6) Loucks, R. G.; Reed, R. M.; Ruppel, S. C.; Hammes, U. *AAPG Bull.* **2012**, *96*, 1071.
(7) Milliken, K. L.; Rudnicki, M.; Awwiller, D. N.; Zhang, T. W. *AAPG Bull.* **2013**, *97*, 177.
(8) Clarkson, C. R.; Freeman, M.; He, L.; Agamalian, M.; Melnichenko, Y. B.; Mastalerz, M.; Bustin, R. M.; Radliński, A. P.; Blach, T. P. *Fuel* **2012**, *95*, 371.
(9) Mastalerz, M.; He, L.; Melnichenko, Y. B.; Rupp, J. A. *Energy Fuels* **2012**, *26*, 5109.
(10) Ruppert, L. F.; Sakurovs, R.; Blach, T. P.; He, L.; Melnichenko, Y. B.; Mildner, D. F. R.; Alcantar-Lopez, L. *Energy Fuels* **2013**, *27*, 772.
(11) Rexer, T. F. T.; Benham, M. J.; Aplin, A. C.; Thomas, K. M. *Energy Fuels* **2013**, *27*, 3099.
(12) Zhang, T. W.; Ellis, G. S.; Ruppel, S. C.; Milliken, K.; Yang, R. S. *Org. Geochem.* **2012**, *47*, 120.
(13) Gasparik, M.; Bertier, P.; Gensterblum, Y.; Ghanizadeh, A.; Krooss, B. M.; Littke, R. *Int. J. Coal Geology* **2014**, *123*, 34.
(14) Ross, D. J. K.; Bustin, R. M. *Mar. Pet. Geol.* **2009**, *26*, 916.
(15) Weniger, P.; Kalkreuth, W.; Busch, A.; Krooss, B. M. *Int. J. Coal Geol.* **2010**, *84*, 190.
(16) Gasparik, M.; Ghanizadeh, A.; Bertier, P.; Gensterblum, Y.; Bouw, S.; Krooss, B. M. *Energy Fuels* **2012**, *26*, 4995.
(17) Chareonsuppanimit, P.; Mohammad, S. A.; Robinson, R. L.; Gasem, K. A. M. *Int. J. Coal Geol.* **2012**, *95*, 34.
(18) Lu, X. C.; Li, F. C.; Watson, A. T. *Fuel* **1995**, *74*, 599.
(19) Chalmers, G. R. L.; Bustin, R. M. *Bull. Can. Pet. Geol.* **2008**, *56*, 22.
(20) Chalmers, G. R. L.; Bustin, R. M. *Int. J. Coal Geol.* **2007**, *70*, 223.
(21) Littke, R.; Baker, D. R.; Leythaeuser, D. *Org. Geochem.* **1988**, *13*, 549.
(22) Vandenbroucke, M.; Behar, F.; Santorcuato, A.; Rullkotter, J. *Org. Geochem.* **1993**, *20*, 961.
(23) Vandenbroucke, M.; Largeau, C. *Org. Geochem.* **2007**, *38*, 719.
(24) Rullkotter, J.; Leythaeuser, D.; Horsfield, B.; Littke, R.; Mann, U.; Muller, P. J.; Radke, M.; Schaefer, R. G.; Schenk, H. J.; Schwochau, K.; Witte, E. G.; Welte, D. H. *Org. Geochem.* **1988**, *13*, 847.
(25) Littke, R.; Leythaeuser, D.; Rullkotter, J.; Baker, D. R. *Geol. Soc. Spec. Publ.* **1991**, *58*, 311−333 (DOI: 10.1144/GSL.SP.1991.058.01.20).
(26) Bernard, S.; Horsfield, B.; Schulz, H.-M.; Wirth, R.; Schreiber, A.; Sherwood, N. *Mar. Pet. Geol.* **2012**, *31*, 70.
(27) Schmid-Rohl, A.; Rohl, H. J.; Oschmann, W.; Frimmel, A.; Schwark, L. *Geobios* **2002**, *35*, 13.
(28) Schwark, L.; Frimmel, A. *Chem. Geol.* **2004**, *206*, 231.
(29) Rohl, H. J.; Schmid-Rohl, A. In *The Deposition of Organic-Carbon-Rich Sediments: Models, Mechanisms, and Consequences*; Harris, N. B., Ed.; SEPM (Society of Sedimentary Geology): Tulsa, OK, 2005; Vol. *82*, p 165.
(30) Munoz, Y. A.; Littke, R.; Brix, M. R. *Geofluids* **2007**, *7*, 335.
(31) Institution, B. S. *BS 733−2:1987: Pyknometers: Methods for calibration and use of pyknometers*; BSI: 1987.
(32) Espitalie, J. *Rev. IFP* **1977**, *32*, 23.
(33) Hillier, S. In *Clay Mineral Cements in Sandstones*; Blackwell Publishing, Ltd.: Malden, MA, 2009; p 213.
(34) Hillier, S. *Clay Min.* **1999**, *34*, 127.
(35) Leon, C. *Adv. Colloid Interface Sci.* **1998**, *76*, 341.
(36) Lapierre, C.; Leroueil, S.; Locat, J. *Can. Geotech. J.* **1990**, *27*, 761.
(37) Heling, D. *Sedimentology* **1970**, *15*, 247.
(38) Lowell, S.; Shields, J. E. *Powder Surface Area and Porosity*; Chapman and Hall: London, New York, 1991.
(39) Lemmon, E. W.; Huber, M. L.; McLinden, M. O. *NIST Reference Fluid Thermodynamic and Transport Properties—REFPROP*; U.S. Department of Commerce: Washington, DC, 2010.
(40) Span, R.; Wagner, W. *J. Phys. Chem. Ref. Data* **1996**, *25*, 1509.
(41) Span, R.; Lemmon, E. W.; Jacobsen, R. T.; Wagner, W.; Yokozeki, A. *J. Phys. Chem. Ref. Data* **2000**, *29*, 1361.
(42) Setzmann, U.; Wagner, W. *J. Phys. Chem. Ref. Data* **1991**, *20*, 1061.
(43) van Krevelen, D.; Schuyer, J. *Coal Science*; Elsevier: Amsterdam, 1957.
(44) Wilhelms, A.; Larter, S. R.; Leythaeuser, D. *Org. Geochem.* **1991**, *17*, 351.
(45) Laxminarayana, C.; Crosdale, P. J. *Int. J. Coal Geol.* **1999**, *40*, 309.
(46) Gurvitch, L. *J. Phys. Chem. Soc. Russ.* **1915**, *47*, 805.
(47) Marsh, H. *Carbon* **1987**, *25*, 49.
(48) Fletcher, A. J.; Thomas, K. M.; Rosseinsky, M. J. *J. Solid State Chem.* **2005**, *178*, 2491.
(49) Sing, K. S. W.; Everett, D. H.; Haul, R. A. W.; Moscou, L.; Pierotti, R. A.; Rouquerol, J.; Siemieniewska, T. *Pure Appl. Chem.* **1985**, *57*, 603.
(50) Garrido, J.; Linares-Solano, A.; Martin-Martinez, J. M.; Molina-Sabio, M.; Rodriguez-Reinoso, F.; Torregrosa, R. *Langmuir* **1987**, *3*, 76.
(51) Marsh, H.; Wynne-Jones, W. F. K. *Carbon* **1964**, *1*, 269.
(52) Sing, K. S. W.; Williams, R. T. *Part. Part. Syst. Charact.* **2004**, *21*, 71.
(53) Lamond, T. G.; Metcalfe, J. E. I.; Walker, P. L. J. *Carbon* **1965**, *3*, 59.
(54) Rodriguez-Reinoso, F.; Linares-Solano, A. In *Chemistry and Physics of Carbon*; Thrower, P. A., Ed.; Marcel Dekker: New York, 1989; Vol. *21*, p 1.
(55) Cazorla-Amoros, D.; Alcaniz-Monge, J.; de la Casa-Lillo, M. A.; Linares-Solano, A. *Langmuir* **1998**, *14*, 4589.
(56) *Handbook of Compressed Gases*, 3rd ed.; Van Nostrand Reinhold: New York, 1990.
(57) Firouzi, M.; Rupp, E. C.; Liu, C. W.; Wilcox, J. *Int. J. Coal Geol.* **2014**, *121*, 123.
(58) Krooss, B. M.; van Bergen, F.; Gensterblum, Y.; Siemons, N.; Pagnier, H. J. M.; David, P. *Int. J. Coal Geol.* **2002**, *51*, 69.
(59) Xiao, B.; Wheatley, P. S.; Zhao, X.; Fletcher, A. J.; Fox, S.; Rossi, A. G.; Megson, I. L.; Bordiga, S.; Regli, L.; Thomas, K. M.; Morris, R. E. *J. Am. Chem. Soc.* **2007**, *129*, 1203.
(60) Lin, X.; Telepeni, I.; Blake, A. J.; Dailly, A.; Brown, C. M.; Simmons, J. M.; Zoppi, M.; Walker, G. S.; Thomas, K. M.; Mays, T. J.; Hubberstey, P.; Champness, N. R.; Schroder, M. *J. Am. Chem. Soc.* **2009**, *131*, 2159.
(61) Furukawa, H.; Miller, M. A.; Yaghi, O. M. *J. Mater. Chem.* **2007**, *17*, 3197.
(62) Murray, L. J.; Dinca, M.; Long, J. R. *Chem. Soc. Rev.* **2009**, *38*, 1294.
(63) Broom, D. P.; Thomas, K. M. *MRS Bull.* **2013**, *38*, 412.
(64) Ambrose, R. J.; Hartman, R. C.; Diaz-Campos, M.; Akkutlu, I. Y.; Sondergeld, C. H. *SPE J.* **2012**, *17*, 219.
(65) Ji, L. M.; Zhang, T. W.; Milliken, K. L.; Qu, J. L.; Zhang, X. L. *Appl. Geochem.* **2012**, *27*, 2533.
(66) Liu, D.; Yuan, P.; Liu, H. M.; Li, T.; Tan, D. Y.; Yuan, W. W.; He, H. P. *Appl. Clay Sci.* **2013**, *85*, 25.
(67) Sircar, S. *Ind. Eng. Chem. Res.* **1992**, *31*, 1813.
(68) Myers, A. L.; Monson, P. A. *Langmuir* **2002**, *18*, 10261.

(69) Cole, J. H.; Everett, D. H.; Marshall, C. T.; Paniego, A. R.; Powl, J. C.; Rodriguez-Reinoso, F. *J. Chem. Soc. Faraday Trans.* **1974**, *70*, 2154.
(70) Czepirski, L.; Jagiello, J. *Chem. Eng. Sci.* **1989**, *44*, 797.
(71) Himeno, S.; Komatsu, T.; Fujita, S. *J. Chem. Eng. Data* **2005**, *50*, 369.
(72) Duren, T.; Sarkisov, L.; Yaghi, O. M.; Snurr, R. Q. *Langmuir* **2004**, *20*, 2683.
(73) Rahman, K. A.; Loh, W. S.; Yanagi, H.; Chakraborty, A.; Saha, B. B.; Chun, W. G.; Ng, K. C. *J. Chem. Eng. Data* **2010**, *55*, 4961.
(74) Ruppel, T. C.; Grein, C. T.; Bienstoc, D. *Fuel* **1974**, *53*, 152.
(75) Xia, X. Y.; Tang, Y. C. *Geochim. Cosmochim. Acta* **2012**, *77*, 489.
(76) Gurdal, G.; Yalcin, M. N. *Int. J. Coal Geol.* **2001**, *48*, 133.
(77) Clarkson, C. R.; Bustin, R. M. *Fuel* **1996**, *75*, 1483.
(78) Clarkson, C. R.; Bustin, R. M.; Levy, J. H. *Carbon* **1997**, *35*, 1689.
(79) Levine, J. R. *Coalification: The Evolution of Coal as Source Rock and Reservoir Rock for Oil and Gas*; American Association of Petroleum Geologists (AAPG): Tulsa, OK, 1993.
(80) Mosher, K.; He, J.; Liu, Y.; Rupp, E.; Wilcox, J. *Int. J. Coal Geol.* **2013**, *109*−*110*, 36.
(81) Cai, Y. D.; Liu, D. M.; Pan, Z. J.; Yao, Y. B.; Li, J. Q.; Qiu, Y. K. *Fuel* **2013**, *103*, 258.
(82) Sing, K. *Colloids Surf., A* **2001**, *187*−*188*, 3.
(83) Mahajan, O. P. *Carbon* **1991**, *29*, 735.